fire

MDPI

Article

Hydrogen in the Natural Gas Network—Relevance for Existing Fire Precautions

Ilian Dinkov *, Jan H. Braun and Dietmar Schelb

Research Centre for Fire Protection Technology, Engler-Bunte-Institute, Combustion Technology Division, Karlsruhe Institute of Technology, 76187 Karlsruhe, Germany; jan.braun@kit.edu (J.H.B.); dietmar.schelb@kit.edu (D.S.)

* Correspondence: ilian.dinkov@kit.edu

Abstract: Power-to-gas technology can be used to convert excess power from renewable energies to hydrogen by means of water electrolysis. This hydrogen can serve as "chemical energy storage" and be converted back to electricity or fed into the natural gas grid. In the presented study, a leak in a household pipe in a single-family house with a 13 KW heating device was experimentally investigated. An admixture of up to 40% hydrogen was set up to produce a scenario of burning leakage. Due to the outflow and mixing conditions, a lifted, turbulent diffusion flame was formed. This led to an additional examination point and expanded the aim and novelty of the experimental investigation. In addition to the fire safety experimental simulation of a burning leakage, the resulting complex properties of the flame, namely the lift-off height, flame length, shape and thermal radiation, have also been investigated. The obtained results of this show clearly that, as a consequence of the hydrogen addition, the main properties of the flame, such as lifting height, flame temperature, thermal radiation and total heat flux densities along the flame, have been changed. To supplement the measurements with thermocouples, imaging methods based on the Sobel gradient were used to determine the lifting height and the flame length. In order to analyze the determined values, a probability density function was created.

Keywords: hydrogen; methane; fire safety; fire precautions

Citation: Dinkov, I.; Braun, J.H.; Schelb, D. Hydrogen in the Natural Gas Network—Relevance for Existing Fire Precautions. *Fire* **2024**, *7*, 189. https://doi.org/10.3390/fire7060189

Academic Editors: Manhou Li and Weiguang An

Received: 22 April 2024
Revised: 28 May 2024
Accepted: 28 May 2024
Published: 4 June 2024

1. Introduction

Mixtures of hydrogen and natural gas are particularly interesting regarding the climate targets of the German government [1]. One reason is that no CO_2 emissions are produced when hydrogen is used to generate energy [2]. In addition, hydrogen can be produced in a climate-neutral way using power-to-gas technologies [3]. Renewable electricity, which is in surplus, can be converted into hydrogen by electrolysis and stored in the gas grid [4,5]. The hydrogen addition is considered a quick solution to decarbonize the heat sector. However, the cost-intensive underutilization of high-quality hydrogen is sometimes viewed critically [6].

According to the rules and regulations of the German Technical and Scientific Association for Gas and Water (DVGW), an admixture of up to 10% hydrogen into the natural gas network is permissible. However, this percentage is to be further increased [4,7]. The Chairman of DVGW, Prof. Dr. Gerald Linke, assumes that a percentage of 20% hydrogen is technically feasible and that transport of more than 50% of green gases is possible [2]. First laboratory tests show that the addition of hydrogen up to 30% can be realized [8,9]. The consequences of higher hydrogen feeds are under investigation in various projects.

One example is the project by E.ON, Avacon and DVGW with a test on the addition of hydrogen to the natural gas network in the Fläming test region. Prior to the start, the gas appliances of the end users were checked and recorded for their hydrogen compatibility. Only four unsuitable appliances were identified among those checked and replaced. During the 2021–2022 heating period, the proportion of hydrogen was gradually increased to 20%.

The functionality of the appliances and emissions were investigated. Of the approximately 350 appliances, 342 were found to have unrestricted functionality. The addition of hydrogen resulted in reductions of CO, NO_X and CO_2 emissions at both full and partial loads. For example, the average reduction in CO emissions was 39% at full load and 5.5% at partial load [8,10].

For further investigation of the hydrogen addition to natural gas, research on the changing properties of methane flames due to hydrogen admixture will be carried out in this work. Aspects relevant to safety and fire protection will also be considered. For the experimental investigation, a testing device was designed, set up and commissioned to simulate an assumed burning leakage within a standard household gas line. The investigated flame was a lifted, turbulent diffusion flame according to the flow and mixture boundary conditions. The resulting flame shape and properties led to an expansion of the aim of the presented study, namely the experimental investigation of the lift-off height, flame length and temperature of the resulting flame at different hydrogen admixtures up to 40%. Experiments were then carried out in order to determine the maximum temperatures and heat flux densities along the vertical burner axis. In addition, two image-based methods are used to determine the lift-off height and the flame length. For this purpose, the recorded videos were evaluated by a human observer and an algorithm. Temperatures along the simulated pipe were also recorded to assess effects that might be relevant to fire protection. While fires/explosions of gas pipes are rather rare, they still occur, as recently observed in Stuttgart, Germany. A gas pipe in front of a building was damaged by the failure of a nearby cable. The subsequent explosion brought the building to a point where it collapsed. Sadly, one person lost his life [11]. It is vital for gas companies and firefighters to Know what they are dealing with. This work will serve as the basis for further investigations on methane-hydrogen flames. Further attention will be paid to fire protection-related aspects in the future.

2. Literature Review on Hydrogen-Natural Gas Mixtures (Summary)

Adding hydrogen to the existing natural gas network is seen as a way to quickly reduce CO_2 emissions from the heating sector [6]. For this reason, this topic is a current subject of research and is being considered in various projects.

When looking at the combustion properties, it became clear that the addition of hydrogen primarily affects the density and calorific value of the fuel gas mixture [12]. It has also been shown that as the hydrogen content increases, the flame length shortens while the combustion temperature increases [12–16]. It has also been shown that the proportions of CO, CO_2 and NO_X emissions change with the addition of hydrogen in contrast to pure methane [13,17,18]. The trend of NO_X emissions is therefore consistent with Zhan et al. [13] and Pignatelli et al. [18]. On the other hand, the development of CO emissions in Pignatelli et al. [18] differs significantly from Zhan et al. [13]. Zhan et al. [13] found an increase in CO emissions significantly below the initial value of pure methane reported by Pignatelli et al. [18]. In El-Ghafour et al. [17], CO emissions initially increase and then decrease from a hydrogen concentration of 30% by volume. One reason for this difference could be the different equivalence ratio. Pignatelli et al. [18] found that as the equivalence ratio increases, the CO concentration decreases in hydrogen-enriched methane flames while increasing in pure methane flames. Furthermore, Pignatelli et al. [18] considered the equivalence ratio for hydrogen-enriched methane flames only up to a value of 0.6, and the further trend of CO emissions is unknown.

The studies considered mainly examined the effect of hydrogen addition on the combustion properties of various burner systems. For the most part, laminar premixed flames were considered. To date, only a few basic studies have been carried out in the area of turbulent diffusion flames. However, in these studies, the focus was mainly on the end use.

This work differs from the presented studies in that it is intended to be a study that is as realistic as possible. It is intended to provide the basis for applied research in the

field of fire protection. For this reason, a burning leakage within a low-pressure pipeline is assumed, which is to be investigated experimentally. In order to investigate this, a testing facility was designed with real boundary conditions regarding mass flow and pressure. The changes in properties such as flame length, heat release, and combustion temperatures are observed in a simulated leak with a lifted, turbulent, non-premixed flame. This means that the focus is more on the question of what changes occur in terms of fire protection and flame properties as a result of adding hydrogen to natural gas than on testing the functionality of the end application [19].

3. Experimental Method

3.1. Scenario

In order to set up a realistic testing device, a scenario was created: a single-family house with a 13 KW heating device had a leak in the pipe—caused, for example, by accidentally drilling into a pipe. The pipes as well as the peripheral devices represented a typical German standard gas system. The gas has an overpressure of 23 mbar in comparison to the environment. The gas pipe had been equipped with a leakage shut-off valve, as has been mandatory in Germany since 2002.

3.2. Experimental Setup

Figure 1 shows a schematic configuration of the experimental setup. A steel plate with gas feed from below is used instead of a pipe so as to simplify measurements. The plate has a length of 1500 mm and a width of 40 mm, roughly half the circumference of a 1-inch gas pipe. The burner is located in the center of the plate and consists of a plenum with a diameter of 30 mm and a length of 100 mm and a nozzle with a diameter of 5 mm. This structure is mounted on an experimental cart made of item profiles. The plate is placed on a small gypsum fiberboard to isolate the item profiles. This permitted free air intake by the burner during the experiments. From below, a pipe leads into the burner. The pressure inside this pipe is measured by a pressure sensor. This pipe is also the outlet pipe of the static mixer. To study the effects caused by the hydrogen addition to natural gas, an ideal premixing (of the two gases) must be performed by the mixer. The methane feed pipe has been inserted into the mixer from the bottom, while the hydrogen pipe has been led in from the bottom side. This arrangement is supposed to create a jet-in-crossflow to mix methane and hydrogen in addition to the static mixer. Right at the mixer, there is a check valve in the methane pipe and one in the hydrogen pipe. These ensure that an operation with only one fuel gas is possible; otherwise one fuel gas could flow into the line of the other fuel gas. The check valves are followed by the respective mass flow controller (MFC) for the fuel gases and, furthermore, by a T-fitting in both lines; the T-fitting allows purging with nitrogen to inert the system. The T-piece is followed by a magnetic valve in each of the gas lines. To prevent the fuel gas from flowing into the nitrogen line, check valves have been installed after the T-pieces. To connect the two nitrogen pipes, another T-piece is used. At the inlet of this T-piece, another magnetic valve has been installed.

During the ignition process, an electric circuit must be bypassed so that the magnetic valves of methane and hydrogen open and the magnetic valve of nitrogen closes. Then, the nitrogen purge is interrupted, and the fuel gases can flow to the burner. A UV flame detector is used to check the ignition. As soon as a flame can be detected, the magnetic valves in the fuel gas pipes remain permanently open, and the magnetic valve in the nitrogen line closes. Table 1 lists the measurement and control equipment used for the investigations.

In order to measure the temperature distribution along the plate, a total of 10 type K thermocouples (TE 1–10) have been attached. Additionally, a heat flux (WF) sensor with a Gardon Gage sensor from Medtherm Corporation has been installed in the plate to record the total heat flux density or a heat flux related to an area [21]. The horizontal distance to the exit nozzle amounts to 10 cm. In addition, another heat flux sensor and a type S thermocouple are placed near the flame (WF 2 and TE 15). The position of the measuring devices can be changed on this holder in a vertical direction in the range of 2.5 cm to

62.5 cm above the outlet so that the temperature and the heat flux density can be recorded over the length of the flame. To record the distance of the thermocouple as well as the heat flux sensor of the nozzle, an additional wire sensor has been installed. The type S thermocouples can be moved horizontally, too. TE 13 and TE 14 observe the temperature of the heat flux sensors. A schematic overview of the location of the thermocouples (red x) and the heat flux sensors (orange) can be found in Figure 2.

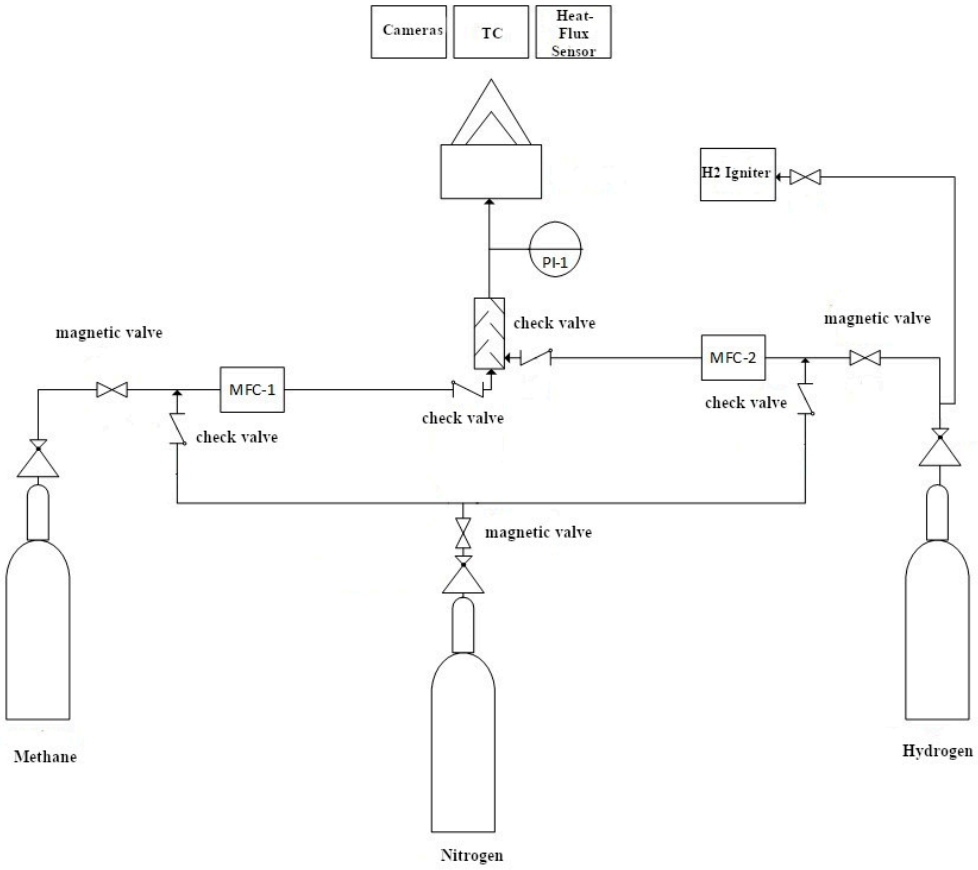

Figure 1. Schematic configuration of the experimental setup.

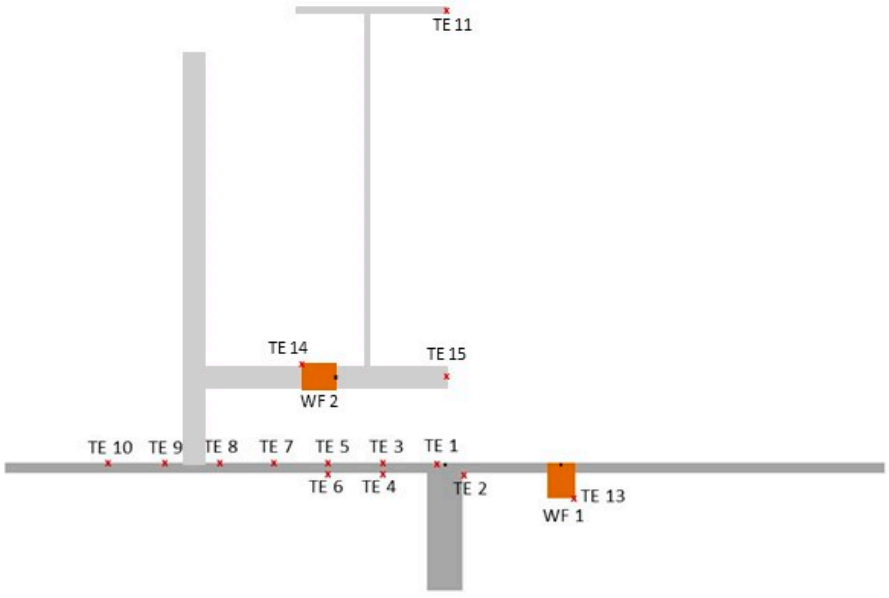

Figure 2. Positions of thermocouples and heat flux sensors.

Table 1. Measurement and control equipment.

Parameter	Measuring and Control Devices	Calibration Range	Position/Exp. Procedure
Pressure	PrimAtü 10	0–120 mbar	S. Figure 1—PI-1/pressure monitoring
Temperature	Thermocouple Type K (NiCr-Ni)	−40–+1200 °C [20]	steel plate, S. Figure 2/temperature distribution along the plate
Temperature	Thermocouple Type S (Pt10%Rh-Pt)	0–+1600 °C [20]	in the flame, S. Figure 2/flame temperatures over the length of the flame, flame length and lift-off height
Heat flux density	Medtherm Corporation Gardon Gage Sensor	0–5 $W \cdot cm^{-2}$	steel plate, S. Figure 2 (WF1)/heat flux near the leakage
Heat flux density	Medtherm Corporation Gardon Gage Sensor	0–10 $W \cdot cm^{-2}$	near the flame, S. Figure 2 (WF2)/heat flux density over the length of the flame
Volume flow rate	Bronkhorst F-201AV-50K-RGD-33-V	0–60 $L \cdot min^{-1}$ H_2	S. Figure 1/volume flow control and monitoring
Volume flow rate	Bronkhorst F-112AC-M20-RGD-33-V	0–100 $L \cdot min^{-1}$ CH_4	S. Figure 1/volume flow control and monitoring

To get an impression of the size of the whole setup, refer to Figure 3a. Figure 3b is a photo taken during an experiment.

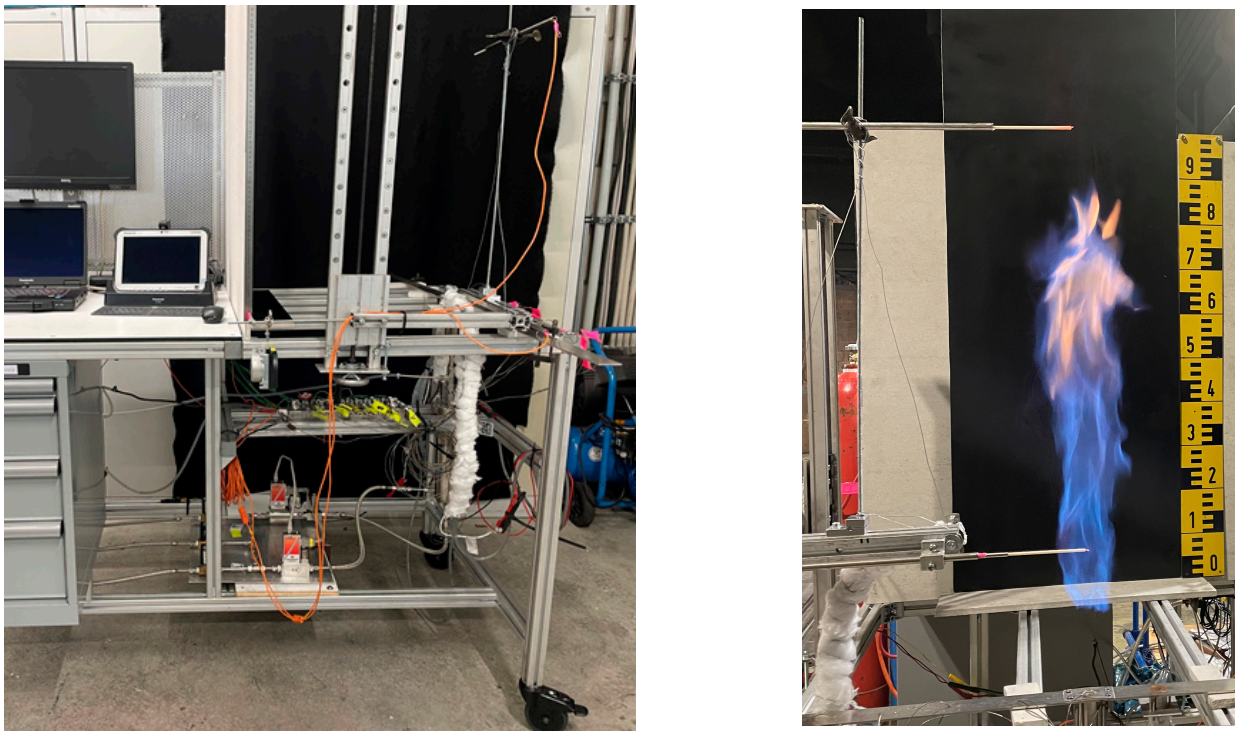

(**a**) (**b**)

Figure 3. Photos of the Experimental Setup. (**a**) Overview, (**b**) Perspective.

3.3. Experimental Procedure

The volume flow rates of 48 $L \cdot min^{-1}$ and 60 $L \cdot min^{-1}$ are analyzed. The volume flow rate of 60 $L \cdot min^{-1}$ is the shut-off point at which a leakage in the scenario would be present. So, in the worst case, the flow rate is just under the maximum flow rate and the valve will not shut off the gas supply. As these shut-off valves have a varying shut-off point, a lower flow rate of 48 $L \cdot min^{-1}$ was tested as well.

Using the measurements with the movable thermocouples and the heat flux sensor, the temperature and the heat flux density over the flame length will be determined. During this process, the temperatures and heat flux densities at the thermocouples, heat flux sensors on the fixture and in the plate, as well as the pressure and position of the measuring equipment on the movable traverse, are recorded in the measuring program. These experiments will be used to determine the temperature distribution along the plate over the complete measurement period and the average heat flux density on the plate over the various hydrogen contents. The temperature profile as well as the heat flux density profile over the height of the flame will also be measured. In addition, the lift-off height is determined. For this purpose, the thermocouple is continuously moved upwards. The point where the temperature gradient is greater than 25 K is defined as the flame start. The temperature measurements are affected by inaccuracies due to the influence of radiation and the heating and cooling in the course of the scenario and were therefore found unsuitable for determining the flame length. For this reason, imaging methods are used to determine the lift-off height and the flame length.

For this purpose, the ignition and setting of the operating point to be investigated are carried out first. Then, the desired hydrogen content is added. After the pressure stabilizes, the camera recording starts. In addition, the flame is also captured by an infrared camera. The operating point is recorded for 1 min. The hydrogen content is increased gradually. This experiment is repeated for all operating points and hydrogen fractions. The cameras are set up at the beginning of the experiments so that the entire flame can be captured on video. This setting is then maintained for all further operating points and not changed to ensure the same camera position as well as the same camera angle for all videos.

Additionally, for the fire safety aspects investigated in this study by a simulation of a leakage in a household pipe, with the installed measurement technique, it was possible to observe the influence of the hydrogen admixture on the main flame properties such as flame shape, length, lift-off height, heat flux, thermal radiation and flame temperature. To supplement the measurements with thermocouples and heat flux density sensors, imaging methods based on the Sobel gradient were used to determine the lifting height and also the flame length of the resulting lifted, turbulent diffusion flame. In order to analyze the determined values, a probability density function was created. An overview of the imaging methods is given in Section 3.4.

3.4. Imaging Methods

The described MATLAB®-algorithm uses a set of functions that will not be discussed in detail, as they are part of MATLAB® itself.

Before the actual algorithm is presented, we'll discuss some of the basics of digital imaging. In this case, the images are saved in the common JPG/JPEG-format, which offers an 8-bit color range, often described as a 24-bit color range or RGB color, as the colors red, green and blue are represented by a value from 0 to 255 each.

The commonly used term "Black-White-Image" usually describes a grayscale image, which has an 8-bit range. An actual "Black-White-Image" features only one bit per pixel. That means pixels only have two states, either 0 (black) or 1 (white).

Below, the algorithm will be described using a highly non-stationary diffusion flame consisting of an 85% methane/15% hydrogen mixture. In this case, the recording was about one minute at 50 frames per second, resulting in at least 3000 frames. The video has a resolution of 3840 × 2160 pixels, which was then cropped to 3840 × 1000 pixels to remove some part of the background to improve the performance of the algorithm. To achieve a high contrast, the recording was made at minimum ambient light. The LEDs in the lower part of the picture are necessary to specify the reference length that is necessary for the algorithm. To describe the algorithm, a single frame of a video will be used. Figure 4 shows the steps of the algorithm.

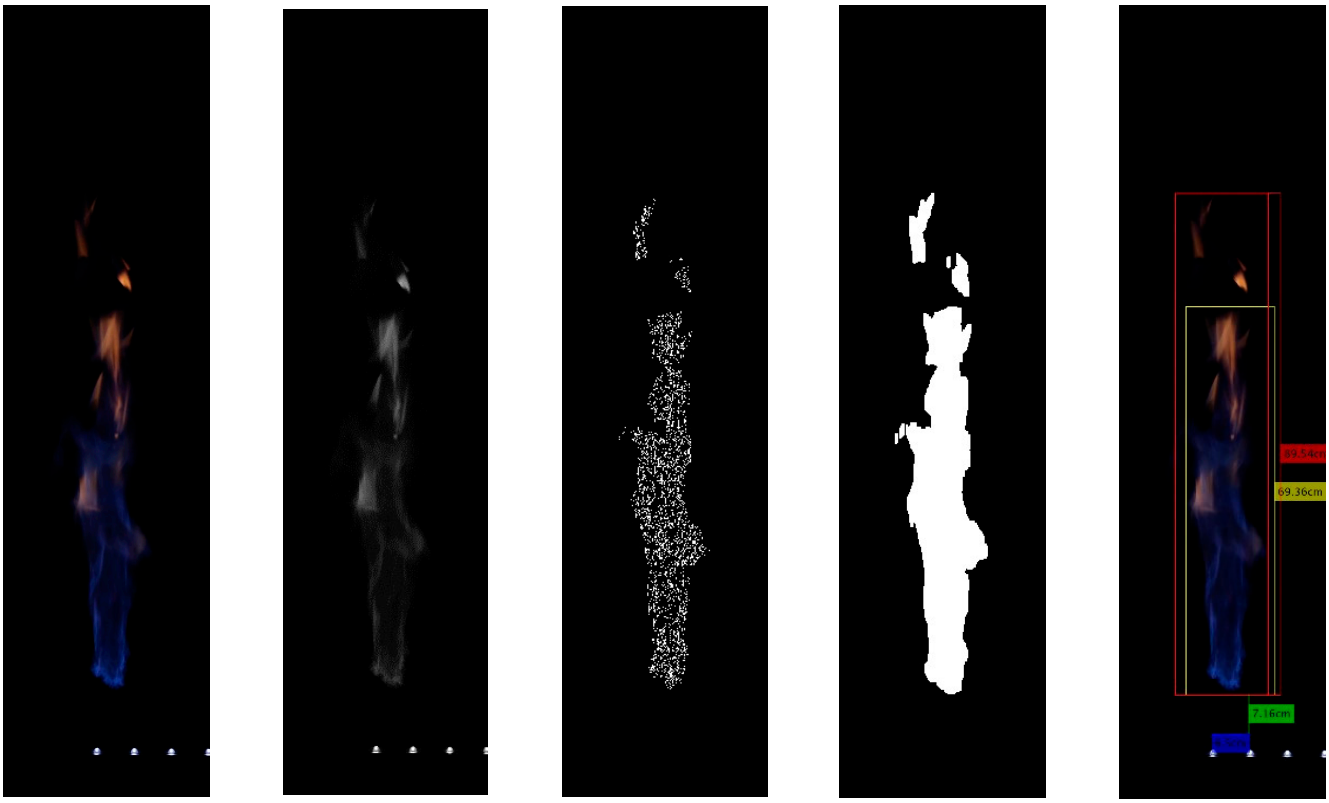

(**a**) (**b**) (**c**) (**d**) (**e**)

Figure 4. Images of the processing; (**a**) Original; (**b**) Converted to grayscale; (**c**) Edge Detection; (**d**) Detected Shape; (**e**) Original Image overlaid with the findings of the Algorithm.

After the images or video are read by the algorithm, it will convert them to grayscale images because the following calculations are easier to perform in grayscale. To represent all parts of brightness, the algorithm performs the grayscale transformation for every pixel with the following coefficients [22]:

$$G = 0.2989 * R + 0.5870 * G + 0.1140 * B \tag{1}$$

That results in Figure 4b.

To further remove potential background effects, the algorithm sets pixels below a specific threshold to 0. Depending on the source image or video, this threshold has to be tweaked by the user.

Now the outer edge of the flame should be recognizable. This is characterized by a gradient, which in this case is from an intensity of 0 to an intensity greater than 0. However, depending on the contrast with the background, a minimum gradient must be specified. This is represented by an image, and thus a two-dimensional intensity matrix, i.e., a two-dimensional gradient, should be used. The decision was made in favor of the Sobel gradient, because it also considers the areas around the respective pixel and gives more weight to the pixels in the respective coordinate direction.

If A is the value of the grayscale image, the values of the gradient for the x-direction and y-direction are given by the following equation [23]:

$$G_x = \begin{bmatrix} +1 & 0 & -1 \\ +2 & 0 & -2 \\ +1 & 0 & -1 \end{bmatrix} * A, \; G_y = \begin{bmatrix} +1 & +2 & +1 \\ 0 & 0 & 0 \\ -1 & -2 & -1 \end{bmatrix} * A \tag{2}$$

The elements of the resulting matrix are now summed up, and the maxima are sought in the image. The matrix obtained in this way now represents a binary image, in which

the recognized edges (maxima of the Sobel gradient) are assigned 1 and everything else is assigned 0. The figure shows many edges because the local maximum is considered in each case and no minimum gradient is specified, which, however, is irrelevant for further processing (Figure 4c).

The algorithm will expand the found edges even more, in this case with one per mil (one percent for low-resolution images) of the resolution in the respective coordinate direction. Due to the high resolution of the images, the overall rather high flame and the small extent of the extension, there is hardly any influence on the edges and thus on the actual shape of the flame. The dilation was implemented as a line for each coordinate direction. This process makes the edges even thicker, which is necessary for the following steps.

Then, the "holes" are filled by setting the areas with the value 0, which are completely surrounded by 1, to 1. This results in connected areas (Figure 4d).

There can still be a few individual fragments of the background. By eroding the image, the edges of the large areas are smoothed, and the small areas disappear. When eroding, the pixels at the edges of the surfaces with a diamond-shaped element of one pixel in each coordinate direction are overwritten with zeros. This step can be repeated several times but should only be taken as often as necessary because the flame in the image will become smaller with each step. Due to the low ambient light here, only two steps were necessary, which resulted in a high accuracy.

Now the object with the greatest circumference can be determined, which, however, does not co-determine the detachment of the flame. The latter must therefore be determined separately by searching for the object or the area with the highest y-value in terms of its extent. If a reference length (blue), in this case the LEDs, is Known, a length-to-pixel ratio can be calculated and used to determine the flame length with (red) and without (yellow) detachments. The reference length also marks the position of the nozzle, and therefore the distance between the nozzle and the flame can be calculated (green) (Figure 4e).

A series of images or a video result in distributions that will be discussed later. To further validate the lift-off height, the lower area of the flame is recorded. For this purpose, an additional ruler has been placed next to the flame so that it can be read off afterwards. During these tests, the lighting was switched on.

4. Results and Discussion

4.1. Temperature

In all tests, the hydrogen content is varied in the range between 0 vol.-% and 40 vol.-% in steps of 5 vol.-%. The ignition was carried out at a volume flow of 10 L·min^{-1} of pure methane for all measurements. Then, the volume flow was increased stepwise to the desired volume flow.

Figure 5 shows the temperature profiles along the nozzle axis of both volume flows for different hydrogen contents. The curves for both volume flows are basically similar. The only difference is that the temperatures are higher at 60 L/min than at 48 L/min. For both volume flows, it is evident that the measurement with 0 vol.-% hydrogen does not record any significant temperature increase up to a certain height. In this range, the flame burns in a lift-off position. From a certain position, a strong increase in temperature can be seen. In the range of 40 cm to 60 cm in height, the temperature reaches its maximum. After that, it starts to decrease again. As the hydrogen content increases, the lift-off height decreases. At 40 vol.-% hydrogen, the flame no longer burns lifted off and the temperature starts to rise right at the beginning. It can also be seen that the maximum temperature is at higher hydrogen concentrations. For this reason, Figure 6 shows the maximum temperatures.

In Figure 6, the maximum temperatures are plotted against the hydrogen fraction. First, the volume flow rate of 48 L·min^{-1} has been analyzed. The maximum temperatures of the three measurements performed are plotted in gray, and the average value of these three measurements is plotted in black. Figure 6a shows that the maximum temperature initially decreases slightly as the hydrogen content increases. At a hydrogen content of

10 vol.-%, the maximum temperature reaches the lowest value of 1456 K. Then, at 15 vol.-% hydrogen, a local maximum of 1500 K can be observed. With further increases in hydrogen content, the maximum temperature remains in the range of about 1490 K. Between a hydrogen content of 30 vol.-% and 35 vol.-%, the maximum temperature rises again and reaches the maximum of 1531 K. Even at a hydrogen content of 40 vol.-%, the maximum temperature remains at this level. In general, an increasing tendency can be seen with increasing hydrogen content. The difference in the maximum temperature between the hydrogen contents of 0 vol.-% and 40 vol.-% is about 40 K, which corresponds to an increase of about 3%. In Figure 6b, the maximum temperature is plotted versus concentration at a volumetric flow rate of 60 L·min^{-1}. Upon closer inspection, it can be observed that the temperature initially decreases with increasing hydrogen content, starting from about 1540 K at 0 vol.-% hydrogen to a minimum of 1499 K at a content of 20 vol.-% hydrogen. As the hydrogen content continues to rise, the maximum temperature also increases. The maximum is reached at a proportion of 40 vol.-% and amounts to approximately 1556 K. Only the temperature at 10% hydrogen by volume is an exception to this trend and is about 5 K higher than the temperature at 5% hydrogen by volume. In general, however, an increasing trend in maximum temperatures between 0 vol.-% and 40 vol.-% hydrogen can also be observed. The difference between these two fractions is about 10 to 15 K (about 0.9%), which is much lower than at a volume flow rate of 48 L·min^{-1}. However, the recorded maximum temperatures for all measured volume fractions are significantly higher at the larger volume flow rate. Basically, the trend is similar for both volume flows. The temperature initially drops to a certain volume fraction before rising further. The adiabatic combustion temperature, which also increases, is cited as the cause of the rising combustion temperature [17].

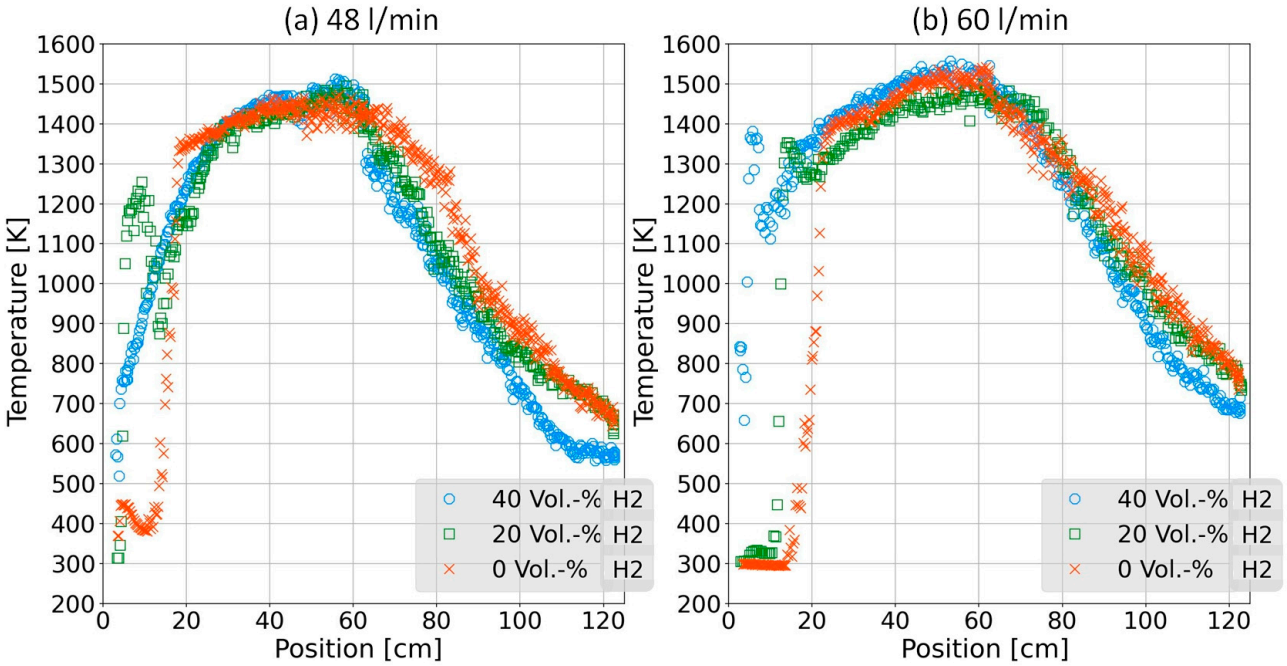

Figure 5. Gas temperature profiles along the nozzle axis.

In addition, the temperatures along the plate were recorded. The duration considered was 25 min, which corresponds to 1500 s. Figure 7 shows the temperature trend along the plate at 60 L·min^{-1} and 0 vol.-% hydrogen as a representative for all measurements. The tendency shown can, in principle, be transferred to all other concentrations. It is particularly noticeable that the temperatures increase especially at thermocouples TE 1 and TE 3. Furthermore, an increase can be detected at TE4. Temperatures seem to stagnate and approach a steady state starting at a time of about 1200 s. In comparison, there was little

to no increase in temperatures at the other thermocouples. The maximum temperature increase of 29.2 K was observed at TE3. The temperature change is negligible at most of the positions of the plate. In general, the temperature increase recorded here does not result in a risk of pipe breakage.

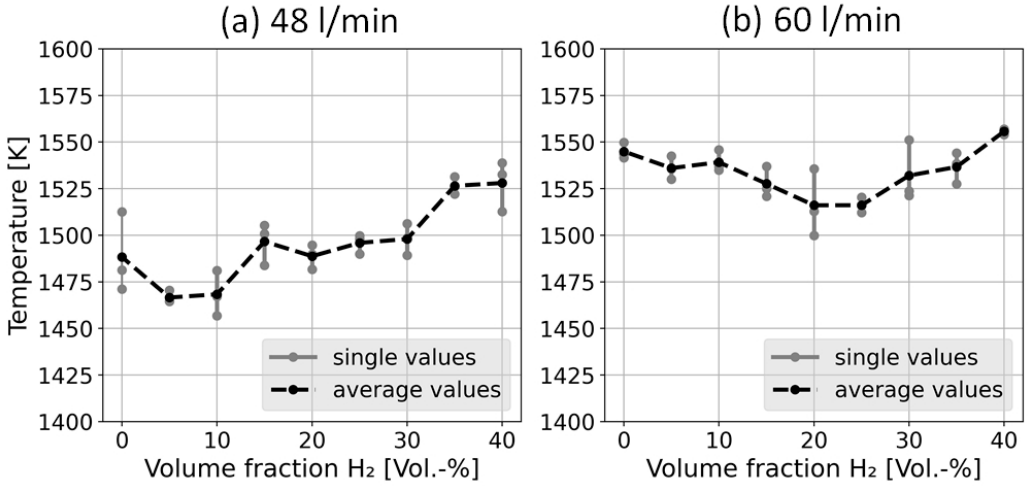

Figure 6. Maximum temperatures for various hydrogen concentrations.

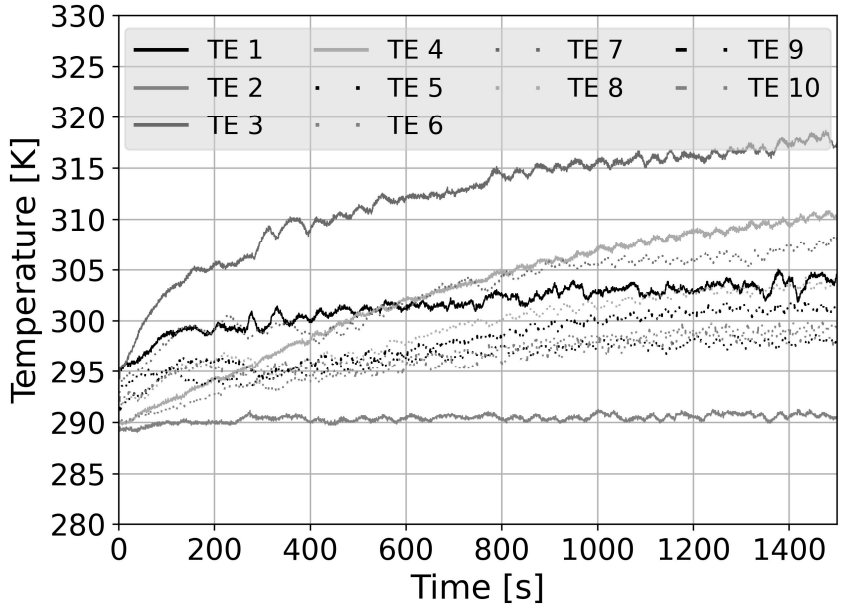

Figure 7. Temperatures at the plate: 60 L·min^{-1}, 0% H_2.

4.2. Heat Flux

In Figure 8, the maximum heat flux densities are plotted on the vertical axis versus the hydrogen concentration. The values are measured along a single vertical line with a horizontal distance of 10 cm. The vertical position of the sensor has been continuously recorded. As shown in Figure 6, the values of the three measurements are plotted in gray and the average values in black.

The volume flow rate of 48 L·min^{-1} in Figure 8a will be discussed first. Generally, the maximum heat flux density decreases with increasing hydrogen content. For example, the difference between the values of 0 vol.-% and 40 vol.-% hydrogen is about 0.03 W·cm^{-2}, which corresponds to a decrease of >7%. Beginning with a hydrogen concentration of 0 vol.-%, the maximum heat flux density decreases up to a concentration of 10 vol.-% hydrogen. At this point, the maximum heat flux density is 0.35 W·cm^{-2}. For the remaining hydrogen fractions, the maximum heat flux density reaches a value of about 0.36 W·cm^{-2},

with the exception of the maximum heat flux density at 35 vol.-% hydrogen. In this case, a maximum heat flux density of about 0.33 W·cm^{-2} has been determined on average. The decreasing tendency can be identified more clearly at a volumetric flow rate of 60 L·min^{-1} in Figure 8b. At this point, the maximum heat flux density decreases by approximately 18% from about 0.49 W·cm^{-2} at 0 vol.-% hydrogen to 0.4 W·cm^{-2} at 40 vol.-% hydrogen. Comparing the two volumetric flows shows that the measured values are significantly higher at the larger volumetric flow rate. Wu et al. [24] found that the total heat flux density increases with increasing hydrogen content due to the higher combustion temperature. However, it was noticeable that the radiative heat flux density decreased due to the higher proportion of hydrogen. The reduced soot concentration and the reduction in CO_2 emissions were cited as the reasons for this [24]. In previous studies at the Karlsruhe Institute of Technology, it was observed that the values recorded by the heat flux sensors that were used agreed very well with the measured values of a radiometer on the same flame [25]. Therefore, it can be assumed that the decreasing heat flux density is due to a reduction of the radiative heat flux density at increased hydrogen contents.

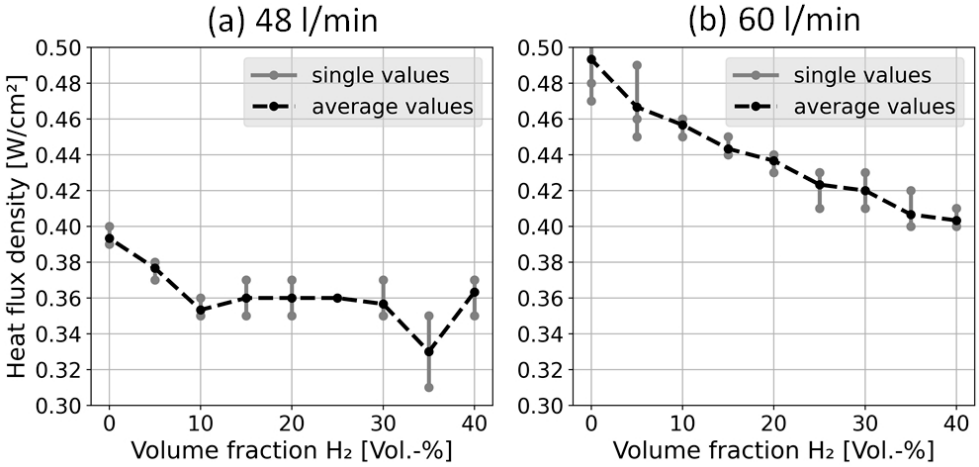

Figure 8. Maximum heat flux densities at the nozzle axis.

4.3. Flame Length

To determine the flame length, a probability density function was created based on the evaluation of the algorithm. For this purpose, the determined flame lengths were divided into 2.5 cm intervals. This is shown in Figure 9.

The corresponding cumulative distribution is shown as a continuous line. The figure shows that with an increased hydrogen content, the probability density function shifts to higher values while also decreasing in wideness. The upper limit of the interval in which the cumulative distribution corresponds to a value of 0.5 then corresponds to the value for the flame length with the related hydrogen content.

Figure 10 shows the optically determined flame lengths. The difference between the two volume flow rates amounts to a maximum of 7.5 cm. Basically, it has been observed that the flame length also increases with the increasing volume fraction of hydrogen. At 48 L·min^{-1}, a slight decrease in flame length can be seen starting at 30 vol.-% hydrogen, but the flame length at 40 vol.-% hydrogen is still 7.5 cm higher than that at 0 vol.-%. The difference in flame lengths between 40 vol.-% and 0 vol.-% hydrogen amounts to 17.5 cm at a volume flow rate of 60 L·min^{-1}. Looking at the video footage, it has been found that the total height from the nozzle to the flame tip decreases with increasing hydrogen content. However, this does not allow any conclusions about the flame length since the lift-off height has been disregarded. The videos show that the lift-off height decreases with the increasing volume fraction of hydrogen. Therefore, it can be determined that the decrease in the lift-off height is greater than the decrease in the total length from the nozzle to the flame tip. This observation partially coincides with the results of El-Ghafour et al. [17]. In this study, it was

generally found that the visible flame length decreases with increasing hydrogen content, but an increase was recorded in the range up to 20 vol.-% compared to the pure methane flame. It also cannot be excluded that a further increase in the hydrogen content results in a shortening of the flame. The shortening of the flame results from the increasing burning speed. Kasabov [26] describes that in this case, the required combustion chamber length was dependent on the flame length, which decreased as a result of the increasing burning speed. From this, it can be deduced that an increase in burning speed leads to a decrease in flame length, which could be observed in our measurements.

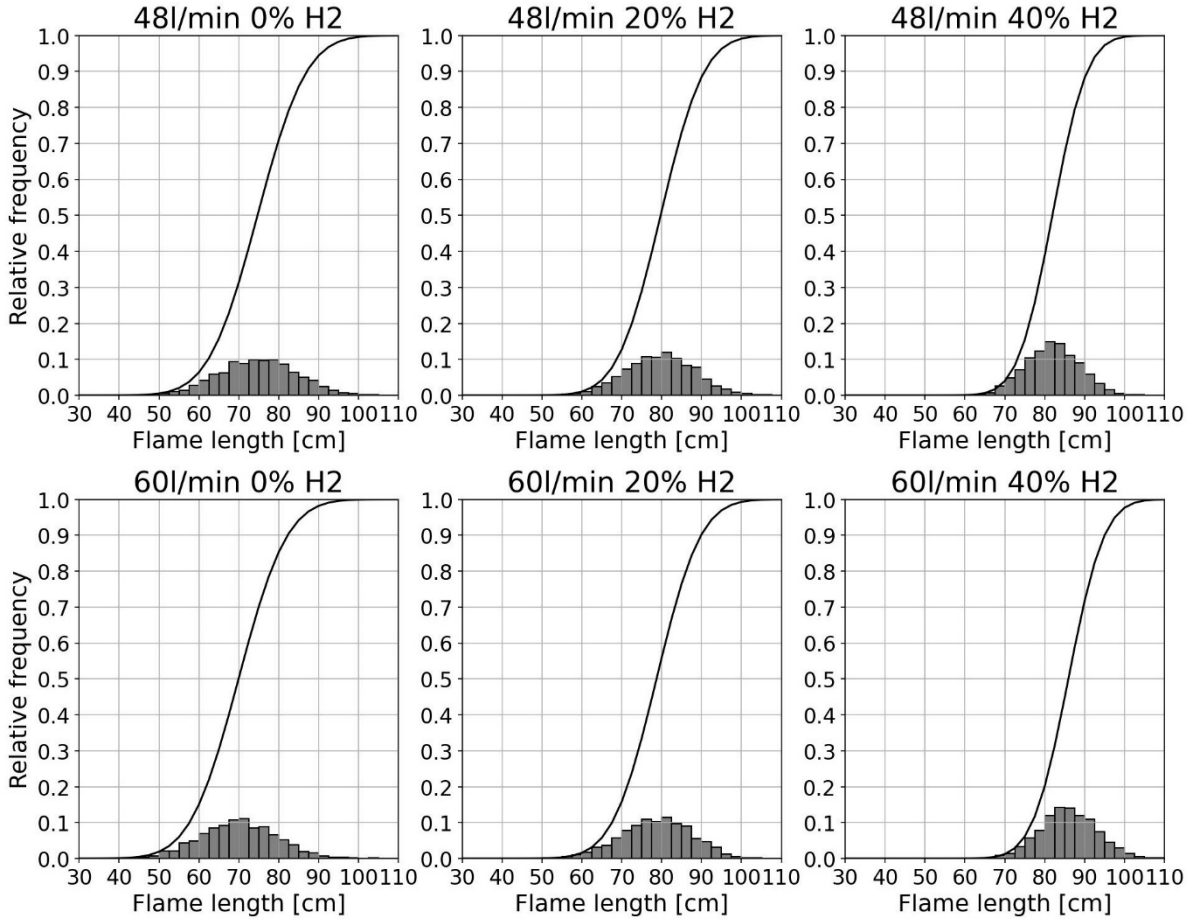

Figure 9. Probability density function of visually determined flame lengths.

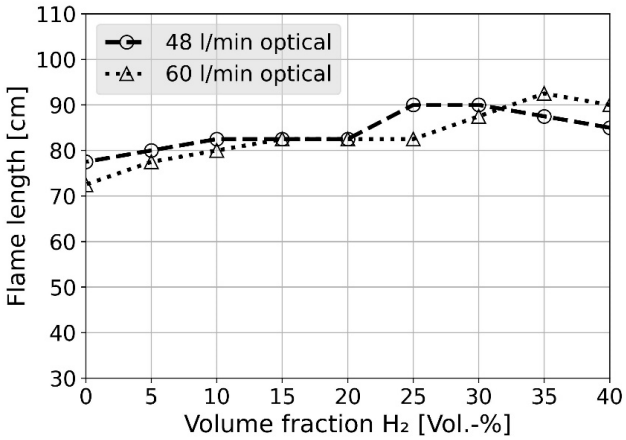

Figure 10. Visually determined flame lengths.

For illustration, Figure 11 shows images of the flames at a volume flow rate of 60 L/min at different hydrogen contents. When comparing the flames shown in Figure 11, it is also evident that the flame diameter becomes smaller as the hydrogen content increases. According to Schumacher and Waldmann [27], the flame diameter depends on the fuel mass flow. As the mass flow rate increases, the diameter also increases. Due to the addition of hydrogen, the density of the fuel mixture decreases. Thus, the fuel mass flow decreases with the hydrogen admixture even though the volume flow remains constant, which then results in a reduction of the flame diameter.

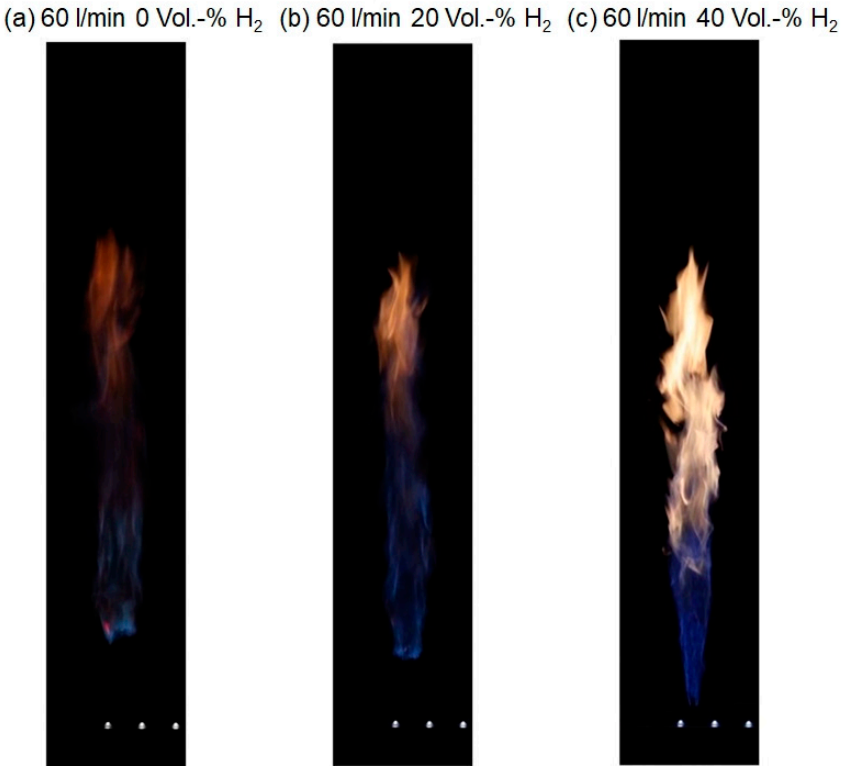

Figure 11. Flame images at a volume flow rate of 60 L/min. (**a**) 0 Vol.-% H_2, (**b**) 20 Vol.-% H_2, (**c**) 40 Vol.-% H_2.

4.4. Lift-Off Height

In Figure 12, the visually determined lift-off heights are plotted against the hydrogen content and compared with the lift-off heights determined with the thermocouple. The determined lift-off heights for both volume flow rates decrease with increasing hydrogen content. The lift-off heights at a volume flow of 60 L·min^{-1} are about 2 to 3 cm higher than at 48 L·min^{-1}, except for the lift-off height at 25 vol.-% hydrogen. Beyond this hydrogen content, the lift-off height at 48 L·min^{-1} can no longer be detected by the algorithm, resulting in a value of 0 cm. The last lift-off height at 60 L·min^{-1} could be detected at a volume fraction of 35 vol.-%, at which the lift-off height is also 0 cm. Comparing the measured lift-off heights with the visually determined ones, it is noticeable that the decrease is almost identical up to a certain concentration. In particular, for a volume flow rate of 48 L·min^{-1} the difference between the two lift-off heights is at most 0.75 cm, up to a volume fraction of 20%. The linear decrease of the lift-off height with increasing hydrogen content is also almost identical up to this point. Only the lift-off height at a hydrogen content of 25 vol.-% is not comparable. Due to the flickering of the flame in this range, the lift-off height cannot be determined exactly by the algorithm, resulting in a value of 0 cm. Considering the volume flow of 60 L·min^{-1}, it is noticeable that the difference between the visually determined and the measured lift-off heights is larger than at 48 L·min^{-1}. Up to a hydrogen content of 25 vol.-%, the trend is basically the same. Both lift-off heights decrease quite linearly with increasing volume fractions. The maximum difference in this range

amounted to 3 cm. Similar to the volumetric flow rate of 48 L·min^{-1} the algorithm can no longer correctly determine the lift-off height above a certain hydrogen content due to flickering. From this point on, the lift-off height decreased more than before until it finally reached 0 cm at 35 vol.-%.

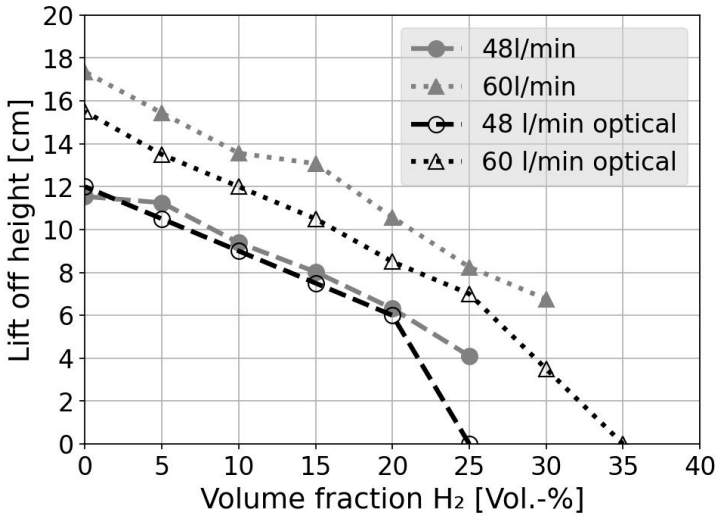

Figure 12. Lift-off heights.

Therefore, measurements were made in which the lift-off height was estimated with the help of a ruler. This is shown in Figure 13. For this purpose, the flame was filmed next to a ruler at 50 frames per second. Ten frames were taken from each of these videos, and the lift-off height was determined for each of these frames. The mean value of these lift-off heights can be found in Table 2.

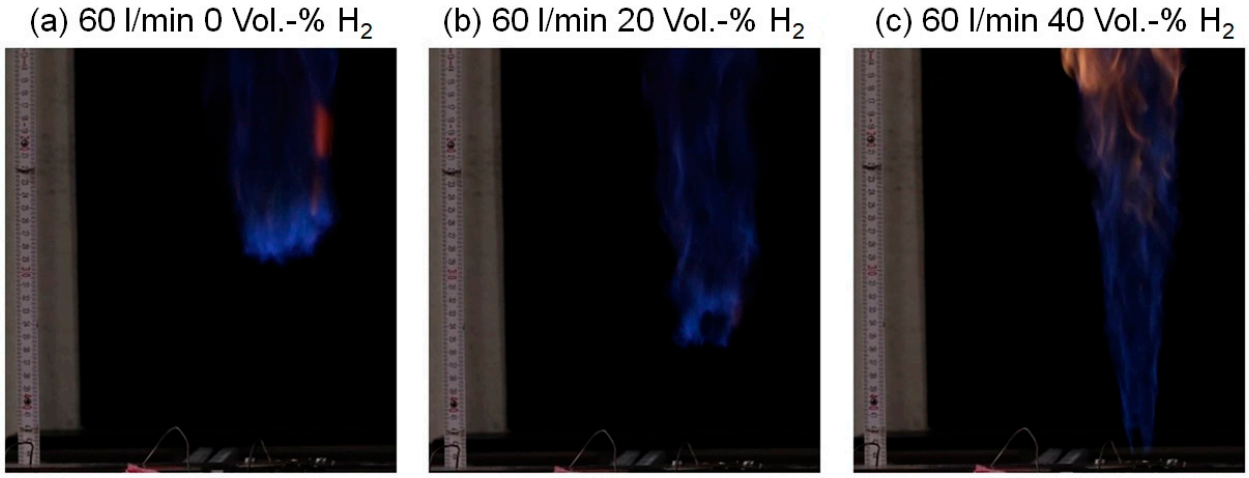

Figure 13. Lift-off heights for different hydrogen fractions at a volume flow rate of 60 L/min. (**a**) 0 Vol.-% H_2, (**b**) 20 Vol.-% H_2, (**c**) 40 Vol.-% H_2.

Basically, the read-off lift-off heights agree quite well with the lift-off heights determined with the help of the thermocouples and optical measurements. Above the area in which the algorithm had problems determining the lift-off height, the lift-off height amounted to a maximum of 1 cm. However, a strong flickering of the flame at the nozzle could be detected.

For the flame to lift off, a certain lift-off velocity has to be exceeded [26,28]. A higher volume flow rate results in a higher flow velocity for the same diameter and parameters. This is why the lift-off height is higher for flames with 60 L·min^{-1}. According to

Sedlmaier [28], the lowering of the lift-off height can be inferred from the increase in turbulent burning velocity. The addition of hydrogen increases the turbulent burning velocity of the flame [29].

Table 2. Lift-off heights estimated with the help of the ruler.

φ_{H_2}	Lift-Off Heights at 48 L·min^{-1} in cm	Lift-Off Heights at 60 L·min^{-1} in cm
0.00	11.1	15.7
0.10	9.9	12.0
0.20	6.2	8.9
0.30	1.0	4.7
0.40	0.3	0.5

5. Visibility/Color

Contrary to expectations, the flame with an increased hydrogen concentration was not less visible, but shone brightly in the range of 30 vol.-% to 40 vol.-% hydrogen admixture. This circumstance was also observed with a further increase in the hydrogen content beyond 50 vol.-% hydrogen (compare also Figure 11). The turnover to a phenomenon resembling the hydrogen flame is in the range of 60 vol.-% to 80 vol.-% hydrogen. Hydrogen emits mainly in the UV range at 300 nm and in the visible range at about 590 nm [30,31]. The radiation in the wavelength range of 500 to 600 nm appears green, yellow and orange, and [31] results from C2 compounds [32]. Due to the increase in the yellow content of the flame, it could be concluded that an increased proportion of C2 compounds has been formed by the hydrogen admixture, up to about 60 to 80 vol.-%. A possible explanation for this phenomenon is that, due to the higher diffusivity and combustion velocity of hydrogen in the lower part of the flame, mainly hydrogen is oxidized.

6. Conclusions

In order to reduce CO_2 emissions while using renewable fuels or CO_2-neutral fuels, an admixture of hydrogen in the natural gas pipelines can be considered a quick solution to decarbonize the heat sector. In this case, hydrogen should be produced in a climate-neutral way while using power-to-gas technologies and renewable electricity to produce hydrogen by electrolysis. Nevertheless, adding hydrogen to natural gas changes the main properties of the reacting gas. It is well Known that hydrogen tends to detonate, while its ignition energy is very low. Considering this, aspects relevant to safety and fire protection should be investigated and taken into account.

The literature overview in Section 2 made it obvious that there is a lack of studies dealing with these aspects. While the combustion behavior of hydrogen is well investigated, regarding main properties like temperatures, emissions and burning velocities, there are only a few publications investigating turbulent, non-premixed flames with hydrogen and methane. Regarding the fire safety aspects of adding hydrogen to natural gas, there are only investigations and tests regarding the functionality of the end applications. The focus of this work is on the question of what changes occur in terms of fire protection and flame properties as a result of adding hydrogen to natural gas.

In the present study, a leak in a household pipe in a single-family house with a 13 KW heating device has been experimentally investigated. An admixture of up to 40% hydrogen was set up to produce a scenario of burning leakage. Due to the outflow and mixing conditions, a lifted, turbulent diffusion flame was formed. A steel plate with gas feed from below was used instead of a pipe so as to simplify measurements. In order to measure the temperature distribution along the steel plate, a total of 10 type K thermocouples have been attached. In addition to the fire safety aspects, including temperatures on the steel plate

near the leakage and flame temperatures by adding hydrogen, flame properties like the flame shape were also an object of investigation.

With the experimental set-up used and especially due to the outflow and mixing conditions, a lifted, turbulent diffusion flame was formed. It was noticeable that the lifting height and the flame length depended on the hydrogen admixture. In the course of the experimental investigations, various combustion properties were investigated, with the main focus being on the effect of hydrogen admixture. The main results of this study are summarized in the subsections below.

Flame temperature

According to the rise in the adiabatic combustion temperature of hydrogen-methane mixtures, the maximum flame temperature increased slightly with an admixture of hydrogen up to 40%. This is also in agreement with other studies cited in Section 2. Furthermore, it has been shown that the maximum measured heat flux densities along the flame axis decreased with an increasing volume fraction of hydrogen. The reason for this can be traced back to the decreasing heat radiation with increasing hydrogen content due to the reduction of soot concentration and CO_2 emissions.

Steel plate temperature and heat flux densities at the nozzle axis

According to the aspects relevant to safety and fire protection, the temperature distribution along the plate as well as the heat flux densities at the nozzle were measured at different hydrogen admixtures. Due to the outflow and mixing conditions, resulting in a lifted flame, the temperature rise as well as the heat flux densities near the nozzle are negligible at most of the positions of the plate. In general, the temperature increase recorded here does not result in a risk of pipe breakage.

Lifting height and flame length

To supplement the measurements with thermocouples, imaging methods were used to determine the lifting height and the flame length. Videos of the various flames were recorded, and 3000 images were evaluated using an algorithm implemented in MATLAB 2024a. The determined values were analyzed using a probability density function. The optical method and the values determined with the thermocouples are in good agreement with each other. It was obvious that an increase in the hydrogen content led to a smaller distribution width. When looking at the flame length, the distribution shifted towards larger values with a higher hydrogen content, while the opposite trend was observed at the take-off height.

Due to the increasing burning rate, a shortening of the flame with increasing hydrogen content was expected. However, it has been shown that the flame length increases in the concentration range of hydrogen, as investigated in this study. This results from the fact that the decrease in the total length from nozzle to flame tip is less than the decrease in the lifting height. With a further increase in the hydrogen content beyond the investigated 40 vol.-%, it can be assumed that the flame length decreases, since the pure hydrogen flame has a very low height.

Emissivity

Contrary to expectations, the flame with an increased hydrogen concentration was not less visible but shone brightly in the range of 30 vol.-% to 40 vol.-% hydrogen admixtures. Due to the increase in the yellow content of the flame, it could be concluded that an increased proportion of C2 compounds has been formed by the hydrogen admixture, up to about 60 to 80 vol.-%. A possible explanation for this phenomenon is that, due to the higher diffusivity and combustion velocity of hydrogen in the lower part of the flame, mainly hydrogen is oxidized.

The results of this study lead to a basic understanding of the changes that come with a hydrogen admixture. It can be used to determine designs for future experiments, for example, the testing of materials.

Author Contributions: Methodology, I.D.; Software, J.H.B.; Formal analysis, I.D.; Investigation, J.H.B.; Data curation, J.H.B.; Writing—original draft, J.H.B.; Writing—review & editing, I.D.; Visualization, J.H.B.; Supervision, I.D. and D.S.; Project administration, I.D. All authors have read and agreed to the published version of the manuscript.

Funding: This paper did not receive external funding.

Data Availability Statement: Data is contained within the article.

Conflicts of Interest: The authors declare no conflict of interest.

References

1. Presse-und Informationsamt der Bundesregierung. Klimaschutzgesetz: Klimaneutralität bis 2045. Bundesregierung. Available online: https://www.bundesregierung.de/breg-de/themen/klimaschutz/klimaschutzgesetz-2021-1913672 (accessed on 22 June 2022).
2. Wächter, S. *Mehr Wasserstoff Technisch Sicher Verankern: DVGW-Regeln für Klimafreundliche Energieinfrastruktur*; Deutsches Verbände Forum: Bonn, Germany, 2019.
3. BDEW. *Was Ist Klimaneutrales Gas? Bio-Erdgas, Synthetisches Gas, Wasserstoff: Heute Klimaschonend, Morgen Klimaneutral*; BDEW: Berlin, Germany, 2020.
4. Tenge, S.; Brandes, A. Erstmals 20 Prozent Wasserstoff im deutschen Gasnetz: Pilotprojekt nimmt Arbeit auf. *DVGW Energ. Wasser-Prax.* **2019**, *12*, 70–71.
5. Schröder, V.; Askar, E.; Tashqin, T.; Habib, A.K. Sicherheitstechnische Eigenschaften von Erdgas-Wasserstoff-Gemischen. 2016. Available online: https://www.bgetem.de/redaktion/arbeitssicherheit-gesundheitsschutz/dokumente-und-dateien/brancheninformationen/energie-und-wasserwirtschaft/gasversorgung/abschlussbericht-zum-forschungsvorhaben-2539-sicherheitstechnische-eigenschaften-von-erdgas-wasserstoff-gemischen (accessed on 15 May 2022).
6. Regulierung von Wasserstoffnetzen Ergebnisse der Marktkonsultation: Zusammenfassung der Stellungnahmen. 2020. Available online: https://www.bundesnetzagentur.de/SharedDocs/Downloads/DE/Sachgebiete/Energie/Unternehmen_Institutionen/NetzentwicklungUndSmartGrid/Wasserstoff/Konsultationsbericht.pdf?__blob=publicationFile&v=1 (accessed on 31 May 2022).
7. Wasserstoff-Beimischung: Sicherheit in Ihrem Zuhause. 2021. Available online: https://www.dvgw.de/medien/dvgw/leistungen/publikationen/sicherheit-h2-beimischung-dvgw.pdf (accessed on 31 May 2022).
8. Erstmals 20 Prozent Wasserstoff im Deutschen Gasnetz: Innovationsprojekt von E.ON, Avacon und DVGW Startet Mit Wasserstoffbeimischung. 2021. Available online: https://www.dvgw.de/medien/dvgw/verein/presse/gempi-dvgw-avacon-eon-beimischung-h2.pdf (accessed on 31 May 2022).
9. Schellhorn, M. Neue Heizgeräte Versprechen Durchbruch Beim Wasserstoff. 2022. Available online: https://www.bundesbaublatt.de/artikel/bbb_Neue_Heizgeraete_versprechen_Durchbruch_beim_Wasserstoff_3735489.html (accessed on 25 July 2022).
10. Dörr, H. Wasserstoff in der Gasinfrastruktur: DVGW/Avacon-Pilotvorhaben mit bis zu 20 Vol.-% Wasserstoff im Erdgas H2-20—Erhebung der Gasinstallationen nach TRGI. 2022. Available online: https://www.dvgw.de/medien/dvgw/meindvgw/fachinfos/forschung/g201902-h2-20-abschlussbericht.pdf (accessed on 31 May 2022).
11. Gaßner, K.M.; Pointner, N. Tote nach Explosion in Stuttgarter Wohnhaus Geborgen. Available online: https://de.nachrichten.yahoo.com/wohnhaus-stuttgart-explosion-teils-eingest%C3%BCrzt-072917986.html?guccounter=1&guce_referrer=aHR0cHM6Ly93d3cuZ29vZ2xlLmNvbS8&guce_referrer_sig=AQAAAIhDgguaC0dNq9rvZ0rJTWrwqwg6lRt8Bn9RBPL13pBGqbq_VBxOAyuBfEVPAzfHIXrn6gvw_Kvq_fBTQfMGigDpJCT8doJkKBevNvpoZT1OJxB9v7dC4coVlzbzYADS_Vr504X8TC62-ArrqL15EKSUGWGqYGBLumakb0Nh2pKu (accessed on 20 May 2024).
12. Lewis, B.; von Elbe, G. *Combustion, Flames and Explosions of Gases*, 3rd ed.; Elsevier: Amsterdam, The Netherlands, 1987.
13. Zhan, X.; Chen, Z.; Qin, C. Effect of hydrogen-blended natural gas on combustion stability and emission of water heater burner. *Case Stud. Therm. Eng.* **2022**, *37*, 102246. [CrossRef]
14. Afgan, N.H. (Ed.) *Heat Transfer in Flames: Selected Chapters from the 1973 Seminar of the International Centre for Heat and Mass Transfer*; Scripta Book Co. u. a: Washington, DC, USA, 1974.
15. Groth, K.M.; Hecht, E.S. HyRAM: A methodology and toolkit for Quantitative Risk Assessment of hydrogen systems. *Int. J. Hydrogen Energy* **2017**, 7485–7493. [CrossRef]
16. Petersen, E.L.; Hall, J.M.; Smith, S.D.; Vries, J.d.; Amadio, A.R.; Crofton, M.W. Ignition of Lean Methane-Based Fuel Blends at Gas Turbine Pressures. *J. Eng. Gas Turbines Power* **2007**, *129*, 937–944. [CrossRef]
17. El-Ghafour, S.; El-dein, A.; Aref, A. Combustion characteristics of natural gas–hydrogen hybrid fuel turbulent diffusion flame. *Int. J. Hydrogen Energy* **2010**, *35*, 2556–2565. [CrossRef]
18. Pignatelli, F.; Kim, H.; Subash, A.A.; Liu, X.; Szasz, R.Z.; Bai, X.S.; Brackmann, C.; Aldén, M.; Lörstad, D. Pilot impact on turbulent premixed methane/air and hydrogen-enriched methane/air flames in a laboratory-scale gas turbine model combustor. *Int. J. Hydrogen Energy* **2022**, *47*, 25404–25417. [CrossRef]
19. Dreyer, L. Wasserstoff im Erdgasnetz Relevanz Für Bestehende Brandschutzmaßnahmen. Master's Thesis, Karlsruhe Institute of Technology Karlsruhe, Germany, 2022.

20. WIKA Alexander Wiegand SE & Co. KG. Einsatz von Thermoelementen, WIKA Datenblatt IN 00.23. 2016. Available online: https://www.wika.com/media/Technical-information/German/ds_in0023_de_de.pdf (accessed on 2 November 2022).
21. Baehr, H.D.; Stephan, K. *Wärme-und Stoffübertragung*; Springer: Berlin/Heidelberg, Germany, 2016.
22. The MathWorks, Inc. 2021. Available online: https://de.mathworks.com/help/matlab/ref/rgb2gray.html (accessed on 20 August 2020).
23. The MathWorks, Inc. 2021. Available online: https://de.mathworks.com/help/images/ref/edge.html (accessed on 15 September 2020).
24. Wu, L.; Kobayashi, N.; Li, Z.; Huang, H. Experimental study on the effects of hydrogen addition on the emission and heat transfer characteristics of laminar methane diffusion flames with oxygen-enriched air. *Int. J. Hydrogen Energy* **2016**, *41*, 2023–2036. [CrossRef]
25. Max, D. Untersuchungen freier Diffusionsflammen mit Propan-Butan Gemisch: VBT-Seminar. Unpublished work. 2022.
26. Kasabov, P. Experimentelle Untersuchungen an Abgehobenen Flammen unter Druck. Ph.D. Thesis, Karlsruhe Institute of Technology, Karlsruhe, Germany, 2014.
27. Schumacher, A.; Waldmann, H. *Wärme-und Strömungstechnik im Dampferzeugerbau: Grundlagen u. Berechnungsverfahren*; Vulkan-Verlag Classen: Essen, Germany, 1972.
28. Sedlmaier, J. Numerische und experimentelle Untersuchung an einer abgehobenen Flamme unter Druck. Ph.D. Thesis, Karlsruhe Institute of Technology, Karlsruhe, Germany, 2019.
29. Fairweather, M.; Ormsby, M.P.; Sheppard, C.; Woolley, R. Turbulent burning rates of methane and methane–hydrogen mixtures. *Combust. Flame* **2009**, *156*, 780–790. [CrossRef]
30. Droste, B.; Eder, A.; Karl, W.; Kesten, M.; Musiol, F.; Rohde, J.; Sauer, G.; Szamer, R.; Ziegler, H.-P. Anwendung der Wasserstoff-Technologie—Eine Bestandsaufnahme: Des Arbeitskreises Wasserstofftechnologie der SFK. 2002. Available online: https://www.kas-bmu.de/sfk-berichte.html?file=files/publikationen/SFK-Publikationen/Berichte/sfk_gs_37.pdf&cid=1664 (accessed on 15 September 2023).
31. Gauglitz, G.; Löbert, H. Einführung in die Spektroskopie, Das elektromagnetische Spektrum und dessen Spektralbereiche. Available online: http://www.chemgapedia.de/vsengine/vlu/vsc/de/ch/13/vlu/spektroskopie/grundlagen/einfuehrung.vlu/Page/vsc/de/ch/13/pc/spektroskopie/grundlagen/spektralbereiche.vscml.html (accessed on 14 November 2022).
32. Lux, J.; Haidn, O. Flame Stabilization in High-Pressure Liquid Oxygen/Methane Rocket Engine Combustion. *J. Propuls. Power* **2009**, *25*, 15–23. [CrossRef]